






Recurrent galactic cosmic-ray flux modulation in L1 and geomagnetic activity during the declining phase of the solar cycle 24

CATIA GRIMANI ^{1,2} ANDREA CESARINI ² MICHELE FABI ^{1,2} FEDERICO SABBATINI,³
DANIELE TELLONI ⁴ AND MATTIA VILLANI ^{1,2}

¹*DiSPeA, University of Urbino Carlo Bo, Urbino (PU), Italy*

²*INFN, Florence, Italy*

³*Alma Mater University, Bologna, Italy*

⁴*National Institute of Astrophysics, Astrophysical Observatory of Turin, Pino Torinese, Italy*

Submitted to ApJ

ABSTRACT

Galactic cosmic-ray (GCR) flux short-term variations (<1 month) in the inner heliosphere are mainly associated with the passage of high-speed solar wind streams (HSS) and interplanetary (IP) counterparts of coronal mass ejections (ICMEs). Data gathered with a particle detector flown on board the ESA LISA Pathfinder (LPF) spacecraft, during the declining part of the solar cycle 24 (February 2016 - July 2017) around the Lagrange point L1, have allowed to study the characteristics of recurrent cosmic-ray flux modulations above 70 MeV n⁻¹. It is shown that the amplitude and evolution of individual modulations depend in a unique way on both IP plasma parameters and particle flux intensity before HSS and ICMEs transit. By comparing the LPF data with those gathered contemporaneously with the magnetic spectrometer experiment AMS-02 on board the International Space Station and with those of Earth polar neutron

monitors, the GCR flux modulation was studied at different energies during recurrent short-term variations. It is also aimed to set the near real-time particle observation requirements to disentangle the role of long and short-term variations of the GCR flux to evaluate the performance of high-sensitivity instruments in space such as the future interferometers for gravitational wave detection. Finally, the association between recurrent GCR flux variation observations in L1 and weak to moderate geomagnetic activity in 2016-2017 is discussed. Short-term recurrent GCR flux variations are good proxies of recurrent geomagnetic activity when the B_z component of the IP magnetic field is directed northern.

Keywords: cosmic ray detectors — interferometers — interplanetary medium — Solar-terrestrial interactions — Heliosphere — Solar rotation

1. INTRODUCTION

The galactic cosmic-ray (GCR) flux at the interstellar medium differs from observations gathered in the inner heliosphere due to a modulation process following the particle propagation through the heliosheath, heliopause and the heliosphere (Florinski et al. 2003). The GCR flux shows a modulation varying with the 11-year solar cycle and the 22-year polarity reversal of the global solar magnetic field (GSMF). This modulation is ascribable to the particle propagation against the outward motion of the solar wind and embedded magnetic field (Balogh 1998). Cosmic rays diffuse, scatter and drift through the solar wind and across inhomogeneities of the interplanetary (IP) magnetic field (Jokipii et al. 1977). Consequently, the cosmic-ray flux modulation in the inner heliosphere appears space, time, charge and energy dependent. Particles with energies below tens of MeV are convected outward before reaching the inner heliosphere while any difference between IP and interstellar GCR energy spectra vanishes above tens of GeV (Florinski & Pogorelov 2009). The GCR proton integral flux above 70 MeV is also observed to decrease by approximately a factor of four with time from solar minimum through solar maximum at 1 AU (Armano et al. 2018a). Spatial variations studied with the PAMELA and Ulysses experiments, for instance, revealed that the GCR intensity increases of

2.7% AU⁻¹ with increasing radial distance from the Sun and decreases of $(0.024 \pm 0.005)\%$ deg⁻¹ with increasing heliolatitude (de Simone et al. 2011). In addition to long-term GCR flux variations, the passage of high-speed solar wind streams (HSS), IP counterparts of coronal mass ejections (ICMEs) and heliospheric current sheet crossing (HCSC) were observed to cause short-term modulations of the overall cosmic-ray flux intensity varying from a few percent to tens percent (McCracken et al. 1966; Armano et al. 2018a, 2019). In particular, during the declining phase of the solar cycle, solar wind streams with speeds $\gg 400$ km s⁻¹, originating from near equatorial coronal holes and equatorward extensions of polar coronal holes, are observed at the ecliptic plane (Tsurutani et al. 2006). HSS generated from coronal holes lasting more than one solar rotation, appear to corotate with the Sun. Fast and slow upstream wind interact generating regions of high-magnetic field compressed plasma called corotating interaction regions (CIRs; Richardson (2004), Armano et al. (2018a) and references therein). The total residence time of cosmic rays in the outer and inner heliosphere is strongly energy dependent and result from longer residence time in the heliotail and heliosheath with respect to that in the heliosphere. The residence time in the heliosphere, in particular, ranges between hundreds of days at 100 MeV n⁻¹ through tens of days above 1 GeV (Florinski & Pogorelov 2009). During this time galactic particles go through HSS and structures in a disturbed IP medium. The most precise data on GCR differential fluxes used to test the particle propagation models in the inner heliosphere are those gathered with magnetic spectrometer experiments consisting of several detectors for redundant particle species selection and energy measurement (see for instance Corti et al. (2019)). Energy differential fluxes from a few tens of MeV through hundreds of GeV measured by the PAMELA and AMS-02 experiments are reported in Martucci et al. (2018); Aguilar et al. (2018). Data gathered monthly are affected by both long and short term modulations (Munini et al. 2018; Adriani et al. 2018; Modzelewska et al. 2019). In particular, recurrent short-term variations appear mainly correlated with HSS transit when cosmic-ray particles undergo diffusion from enhanced IP magnetic field and convection in the solar wind (Sabbah 2000). Long and short-term GCR flux variations are observed to be energy dependent with particle spectra being more depressed at hundreds

of MeV with respect to GeV energies. Moreover, short-term modulation of the GCR flux is strongly space dependent (Benella et al. 2020).

This work focuses on cosmic-ray protons and helium observations gathered above 70 MeV n^{-1} with a particle detector (PD) placed on board the European Space Agency (ESA) LISA Pathfinder spacecraft (Antonucci et al. 2011, 2012; Armano et al. 2016, 2018b) orbiting around the Lagrange point L1 at 1.5×10^6 km from Earth between February 2016 and July 2017. The years 2016-2017 belonged to the declining phase of the solar cycle 24, characterized by a positive epoch of the GSMF (defined by the solar magnetic field directed outward at the Sun north pole (Armano et al. 2018a, 2019)). The role of isolated and interplaying IP structures in modulating the cosmic-ray flux as a function of the energy is discussed here by comparing the LPF data with those gathered during the same period of time above 450 MeV n^{-1} by the AMS-02 magnetic spectrometer experiment hosted on board the International Space Station (ISS; Aguilar et al. (2018)) and with those from polar neutron monitors (www.nmdb.eu). It is observed that similar interplanetary structures produce different effects on cosmic rays. In Armano et al. (2018a, 2019); Grimani et al. (2019b) we carried out an attempt to interpolate the energy differential fluxes of the GCRs just before and at the dip of Forbush decreases (FDs) (Forbush 1937, 1954, 1958; Cane 2000), sudden drops of the GCR intensity associated with the passage of ICMEs and shocks, with the aim of providing empirical relationships on the flux variation during the event evolution. A similar approach is adopted in this work for recurrent GCR flux variations. The outcomes of this work and data from cosmic-ray and solar physics experiments will be used to study the LISA (Amaro-Seoane et al. 2017) mission noise force induced by the charging process on the gold-platinum free-falling test masses (Grimani et al. 2015). In particular, lessons learned with LPF about the relevant role of GCR short-term variations in generating low-frequency noise associated with the test-mass charging process indicate that a continuous monitoring of the energy dependence of GCR short-term variations on board space interferometers will be mandatory (Armano et al. 2017; Villani et al. 2020). Energy, space and time short-term variations of the GCR flux will be monitored with particle detectors placed on board the LISA spacecraft and neutron monitor observations. Galactic cosmic-ray short-term variations will be also considered to estimate

the varying background noise on the visible and ultraviolet images of Metis, the coronagraph flown on board the ESA-NASA (National Aeronautics and Space Administration) Solar Orbiter launched from Cape Canaveral on February 9, 2020 (Andretta et al. 2014; Telloni et al. 2016; Antonucci et al. 2019). Finally, recurrent GCR flux depressions observed in L1 allow for monitoring HSS passage at the origin of geomagnetic disturbances of weak to moderate intensity (Tsurutani et al. 2006).

2. THE PARTICLE DETECTOR ON BOARD LISA PATHFINDER

The LPF spacecraft was launched from the Kourou base in French Guiana on December 3, 2015 on board a Vega rocket. The spacecraft reached its operational six month orbit around the Earth-Sun Lagrangian point L1 at 1.5 million km from Earth (in the Earth-Sun direction) at the end of January 2016. The LPF elliptical orbit was inclined at about 45 degrees with respect to the ecliptic plane. Orbit minor and major axes were approximately of 0.5 million km and 0.8 million km, respectively. The spacecraft spinned around its own axis in approximately six months. The LPF satellite carried two, nearly 2 kg cubic gold-platinum free-floating test masses that played the role of mirrors of the interferometer. Protons and nuclei with energies larger than 100 MeV n^{-1} penetrated or interacted in 13.8 g cm^{-2} of spacecraft and instrument material thus charging the LPF test masses. The test-mass charging due to galactic and solar energetic particles (SEPs) results in noise force limiting the sensitivity of space interferometers mainly below 1 mHz (Armano et al. 2017). As a result, a PD (Canizares et al. 2011) was placed on board LPF to monitor the overall incident GCR and solar particle fluxes (Shaul et al. 2006). The PD was mounted on a honeycomb satellite wall at about one meter distance from test masses and surrounding instrumentation in order to limit the impact of secondary particles in affecting the response of the instrument (Araujo et al. 2005; Armano et al. 2018c). The PD viewing axis was oriented along the Sun-Earth direction. The detector consisted of two $\sim 300 \mu\text{m}$ thick silicon wafers of $1.40 \times 1.05 \text{ cm}^2$ area each, separated by 2 cm and placed in a telescopic arrangement. For particles with energies $> 100 \text{ MeV n}^{-1}$ and an isotropic incidence, the instrument geometrical factor was found to be energy independent and equal to $9 \text{ cm}^2 \text{ sr}$ for each silicon layer. The total geometrical factor for particle counting was $17 \text{ cm}^2 \text{ sr}$. In coincidence mode (particles traversing both silicon wafers), the geometrical factor was $0.9 \text{ cm}^2 \text{ sr}$. The silicon wafers

were placed inside a shielding copper box of 6.4 mm thickness meant to stop particles with energies below 70 MeV n^{-1} . The PD allowed for the counting of protons and helium nuclei traversing each silicon layer and for the measurement of ionization energy losses of particles in coincidence mode. The maximum allowed detector counting rate was $6500 \text{ counts s}^{-1}$ on both silicon wafers, corresponding to an event integrated proton fluence of $10^8 \text{ protons cm}^{-2}$ at energies $> 100 \text{ MeV}$. In coincidence mode up to 5000 energy deposits per second could be stored on the on board computer. Particle counts only were used for the analysis presented in this work (the corresponding instrument GF was $17 \text{ cm}^2 \text{ sr}$). Particle ionization energy losses would have been used for SEP evolution monitoring. No SEP events were observed during the LPF mission operations with associated proton fluences above a few tens of MeV n^{-1} overcoming that of GCRs.

3. GALACTIC COSMIC-RAY FLUX VARIATIONS WITH TIME

A continuous monitoring of long and short-term variations of cosmic rays of galactic origin was allowed during the LPF mission elapsed time.

3.1. *Long-term variations*

Long-term variations of the GCR flux are those characterized by durations $> 1 \text{ year}$. The GCR flux modulation associated with the eleven year solar cycle and the twenty-two year GSMF polarity change are widely studied in the literature both on Earth with neutron monitors (NMs; see for instance [Storini \(1990\)](#)) and in space with balloon ([Shikaze et al. 2007](#)) and satellite experiments ([Potgieter 2013](#)). The monthly averaged sunspot number (SSN; www.sidc.be/silso/datafiles_old) is the most widely used proxy to monitor the variations of the solar activity correlated with the solar modulation parameter within the symmetric model of GCR energy spectra in the force-field approximation by Gleeson and Axford (G&A; [Gleeson & Axford \(1968\)](#)). This model allows to estimate the cosmic-ray intensity in the inner heliosphere by assuming an interstellar energy spectrum and a solar modulation parameter that basically represents the energy loss of cosmic rays while propagate from the interstellar medium to the point of observations. The G&A model is found to reproduce the GCR measurements at 1 AU in the energy range from tens of MeV to hundreds of GeV during GSMF pos-

itive polarity epochs (Grimani et al. 2007). It is worthwhile to point out that different values of the solar modulation parameter are set when data are compared to model predictions if different GCR energy spectra at the interstellar medium are considered. Voyager 1 measured the interstellar spectra of ions and electrons below 1 GeV (Stone et al. 2013), however, the solar modulation parameter reported in http://cosmicrays oulu.fi/phi/Phi_mon.txt, was estimated according to the Burger et al. (2000) interstellar proton spectrum (Usoskin et al. 2011). Therefore, solar modulation parameter and interstellar particle spectra must be properly adopted. The G&A model takes into account particle diffusion and convection processes, however during negative (positive) polarity periods of the GSMF, positive (negative) GCR particles undergo also a global drift motion from the solar equator (poles) towards the poles (equator). Positive (negative) particle fluxes are more modulated during negative (positive) polarity periods and a larger solar modulation is estimated with respect to an analogous solar modulation during a positive polarity epoch (Grimani et al. 2007). As a result, the monthly solar modulation parameter reported in http://cosmicrays oulu.fi/phi/Phi_mon.txt is representative of the overall effects of long and short GCR flux variations (Usoskin et al. 2017). This empirical approach allows us to make average predictions of the GCR flux when the solar activity is known (see Armano et al. (2019)). However, to study the performance of very sensitive instruments, for instance, the role of short term variations must be considered separately from the long term ones. Observations carried out with the BESS (Shikaze et al. 2007) magnetic spectrometer experiment flown on balloons several times during more than one solar cycle after 1997 allowed to investigate the energy dependence of the solar modulation and solar polarity inferred from proton and helium differential fluxes. More recently, the experiments AMS-01 on the Space Shuttle Discovery (AMS Collaboration et al. 2002), PAMELA on a satellite (Pamela Collaboration et al. 2017) and AMS-02 on the International Space Station (ISS) (Aguilar et al. 2018) provided continuous cosmic-ray data monitoring in space in the last 15 years. PAMELA was launched in 2006 and remained into a quasi-polar elliptical orbit around the Earth between the end of the solar cycle 23 and the solar cycle 24, mostly during a negative polarity period. AMS-02 was installed in 2011 on the ISS and gathered data for the majority of time during a positive polarity epoch after the last polarity change

from - to + at the end of 2013. PAMELA observations extended down to 70 MeV n^{-1} and allowed for monitoring the most populated region of the GCR energy spectrum which is a fundamental requirement for monitoring short-term GCR flux variations, while AMS-02 provided data above 450 MeV n^{-1} due to the shielding effect of the geomagnetic field along the ISS orbit. PAMELA GCR short-term variation observations were reported for instance in [Adriani et al. \(2011\)](#); [Munini et al. \(2018\)](#); [Adriani et al. \(2018\)](#); [Modzelewska et al. \(2019\)](#). Unfortunately, it was not feasible for us to infer from paper figures the energy dependence of individual GCR flux short-term variations on time scales of hours or days at the most.

A decreasing solar activity was observed during the LPF mission elapsed time when the monthly averaged sunspot number varied from 56 in February 2016 through 18 in July 2017 ([Armano et al. 2018a](#)). During this same period the solar modulation parameter and the LPF cosmic-ray PD counting rate varied from 468 MV/c through 383 MV/c (http://cosmicrays oulu.fi/phi/Phi_mon.txt) and from about 120 counts through over 150 counts every 15 seconds, respectively, revealing an average increase of 20% of the GCR proton and helium flux intensity above 70 MeV n^{-1} ([Armano et al. 2018a](#); [Grimani et al. 2019a](#)).

3.2. *Short-term variations*

GCR flux short-term variations are characterized by durations < 1 month and result associated with the transit of HSS and IP structures. The GCR flux short-term variations can be either recurrent and non-recurrent.

The first kind is mainly associated with CIRs generated by HSS originating from coronal holes and overtaking leading slow solar plasma ([Richardson 2004](#)). Recurrent GCR flux short-term variations present the same periodicities of the Sun rotation period and higher harmonics (see for instance [Armano et al. \(2018a\)](#)).

Intense non-recurrent GCR flux drops associated with ICME and shock transit are known as FDs. These short-term GCR flux depressions show up to 25% intensities in Earth neutron monitors ([Benella et al. 2020](#)).

GCR recurrent and non recurrent short-term variations have been widely studied in the last sixty years with Earth neutron monitors (Forbush 1954, 1958; Cane 2000). However, in Armano et al. (2018a, 2019) it was pointed out that the whole evolution of weak Forbush decreases and recurrent variations showing intensities $< 10\%$ in space cannot be studied with neutron monitors measurements that appear modulated by $< 3\%$. As a matter of fact, neutron monitor observations are sensitive to secondary particles generated by primaries incident at the top of the atmosphere with energies above 500 MeV but vary of the same amount of the GCR integral flux, thus providing a direct measurement of the same, at energies above *effective energies* (which range between 11-12 GeV and above 20 GeV for near-polar and equatorial stations, respectively; see Gil et al. (2017)). Noteworthy, a large sample of data below 100 MeV/n will be available soon with the EPD (Energetic Particle Detector; Rodriguez-Pacheco et al. (2019)) on board Solar Orbiter for instance. Unfortunately, the small geometrical factor in the cosmic-ray energy range limits the capability of this instrument to follow the dynamics of the GCR flux short-term variations smaller than one day.

4. GCR FLUX RECURRENT DEPRESSIONS AND INTERPLANETARY PLASMA PARAMETERS DURING THE LISA PATHFINDER ELAPSED TIME

The LPF hourly averaged proton and helium integral flux measurements above 70 MeV n^{-1} were characterized by statistical uncertainties of 1% over the entire mission duration. In order to limit the effect of the solar modulation decrease in 2016-2017, the percent variations of these data were calculated with respect to the average value observed during each Bartels rotation (BR) through the whole period of the mission operations (see Armano et al. (2018a)). It is recalled here that the BR number corresponds to the number of 27-day rotations of the Sun since February 8, 1832 (Armano et al. 2018a; Benella et al. 2019b,a). Data gathered during the BRs 2493, 2494, 2500 and 2503 are reported in the following. The LPF data revealed that above 70 MeV n^{-1} the monthly GCR flux varied up to 15% during the BR 2496 (Armano et al. 2018a; Grimani et al. 2019b). A similar overall GCR flux decrease is observed when the solar modulation parameter increases by about 100 MV/c. As a result, it is important to disentangle the role of long and short-term cosmic-ray variations. Forty-five GCR flux recurrent variations were observed during the LPF mission elapsed

time from March 2016 (BR 2491) through July 2017 (BR 2509). In Fig. 1 the LPF GCR percent flux variations during the BR 2493 (April 27, 2016 - May 23, 2016) are compared to contemporaneous IP plasma parameter and magnetic field data. The association between GCR flux drops and solar wind speed increase at the passage of HSS is observed all through the data sample (see [Richardson et al. \(1996\)](#) for instance for a previous study). The following criteria for selecting the GCR recurrent depressions observed on board the LPF spacecraft were applied: 1) depression commencements were set at the beginning of each continuous decrease of the GCR flux observed for more than 12 hours; 2) the whole duration was > 1 day and 3) the amplitude was $> 1.5\%$. In general, the peaks of the GCR flux are observed when the solar wind speed presents values smaller than 400 km s^{-1} and the IP magnetic field remains below 10 nT ([Armano et al. 2018a, 2019](#); [Grimani et al. 2019b](#)). However, even when the above IP parameters are higher than the indicated values and the GCR flux appears modulated, the amplitude of the modulation appears different depending on the GCR flux intensity before the perturbation and on the interplay of subsequent HSS. For instance, the decrease of the GCR flux between May 7 and May 9, 2016 in Fig. 1 was of 5% due to a solar wind increase of about 300 km s^{-1} from about 400 km s^{-1} through 700 km s^{-1} . A double decrease is observed between May 16 and May 21, 2016 with a solar wind increase of less than 200 km s^{-1} above 400 km s^{-1} . The difference is ascribable to the pre-HSS passage intensity of the GCRs: compatible with the average value observed during the whole BR 2493 in the first case and equal to the maximum value observed during the same BR in the second case. Maximum and minimum variations with respect to monthly averages observed during the mission operations were $+9\%$ and -7% observed during the BR2495 and BR2502, respectively. The role of interplaying structures can be observed by comparing Figs. 1 and 2 where the LPF GCR data during the BRs 2493 and 2494 are shown. The last week of these two BRs is characterized by a GCR flux depression beginning on May 16-17 during the BR 2493 and June 12-13 during the BR 2494. The decrease phase is associated with the transit of recurrent HSS. During the BR 2493 the GCR flux is observed to recover after one-day *plateau* ([Armano et al. 2018a](#)) because the speed of the solar wind goes down to $\simeq 400 \text{ km s}^{-1}$ while during the BR 2494 the GCR flux recovery phase is disturbed for 6 days by the passage of several superposing HSS with the solar

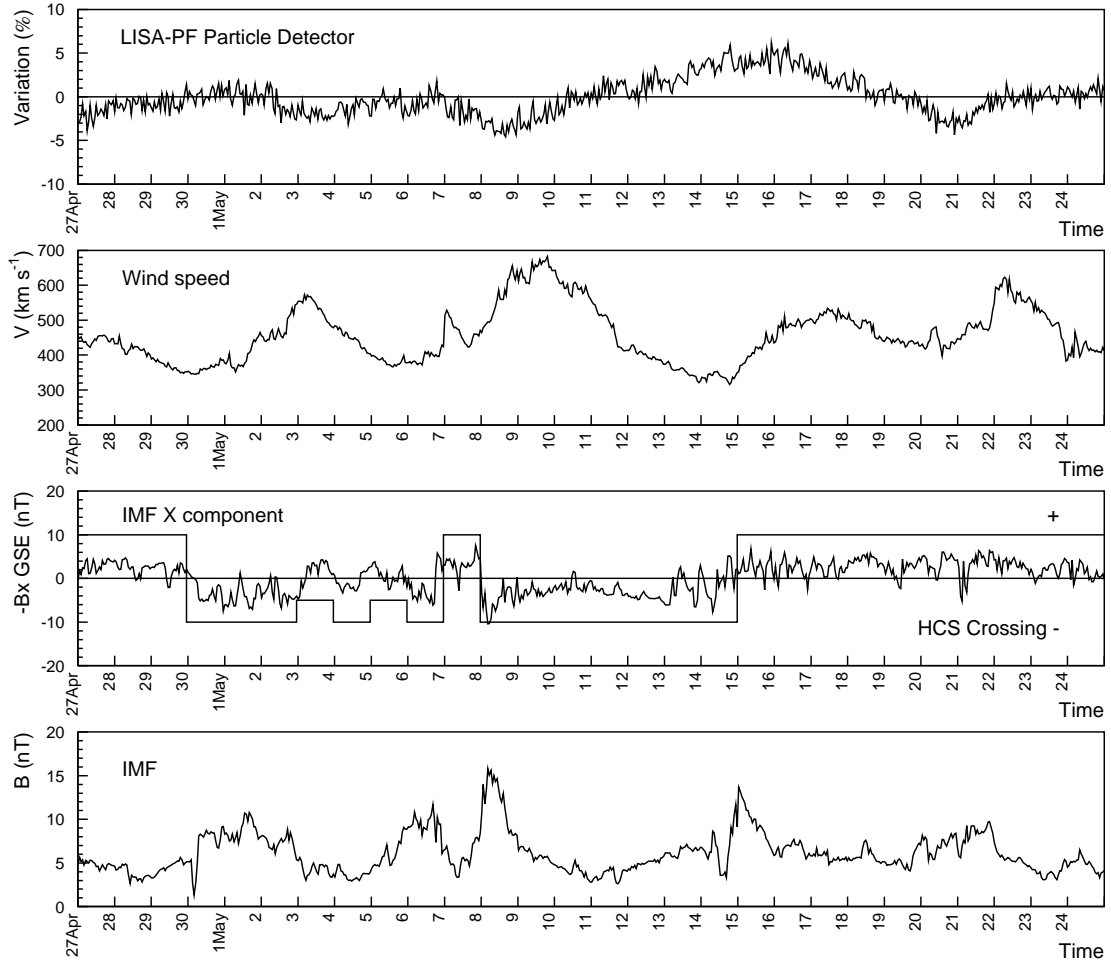


Figure 1. LPF PD counting rate percent variations during the BR 2493 (April 27, 2016 - March 23, 2016; first panel). Solar wind speed (second panel), IMF radial component (third panel) and IMF intensity (fourth panel) contemporaneous measurements, gathered by the ACE experiment, are also shown. HCS crossing (http://omniweb.sci.gsfc.nasa.gov/html/polarity/polarity_tab.html) is indicated in the third panel.

wind speed remaining well above 400 km s^{-1} . The energy dependence of the GCR flux variations is inferred from Figs. 3 and 4 and Table 1 from the comparison of GCR flux decreases observed with LPF during the BR 2493 and BR 2494 above 70 MeV n^{-1} to contemporaneous hourly averaged polar neutron monitor measurements representing the GCR flux variations above the effective energy of 11 GeV (see [Armano et al. \(2018a\)](#) and references therein for details).

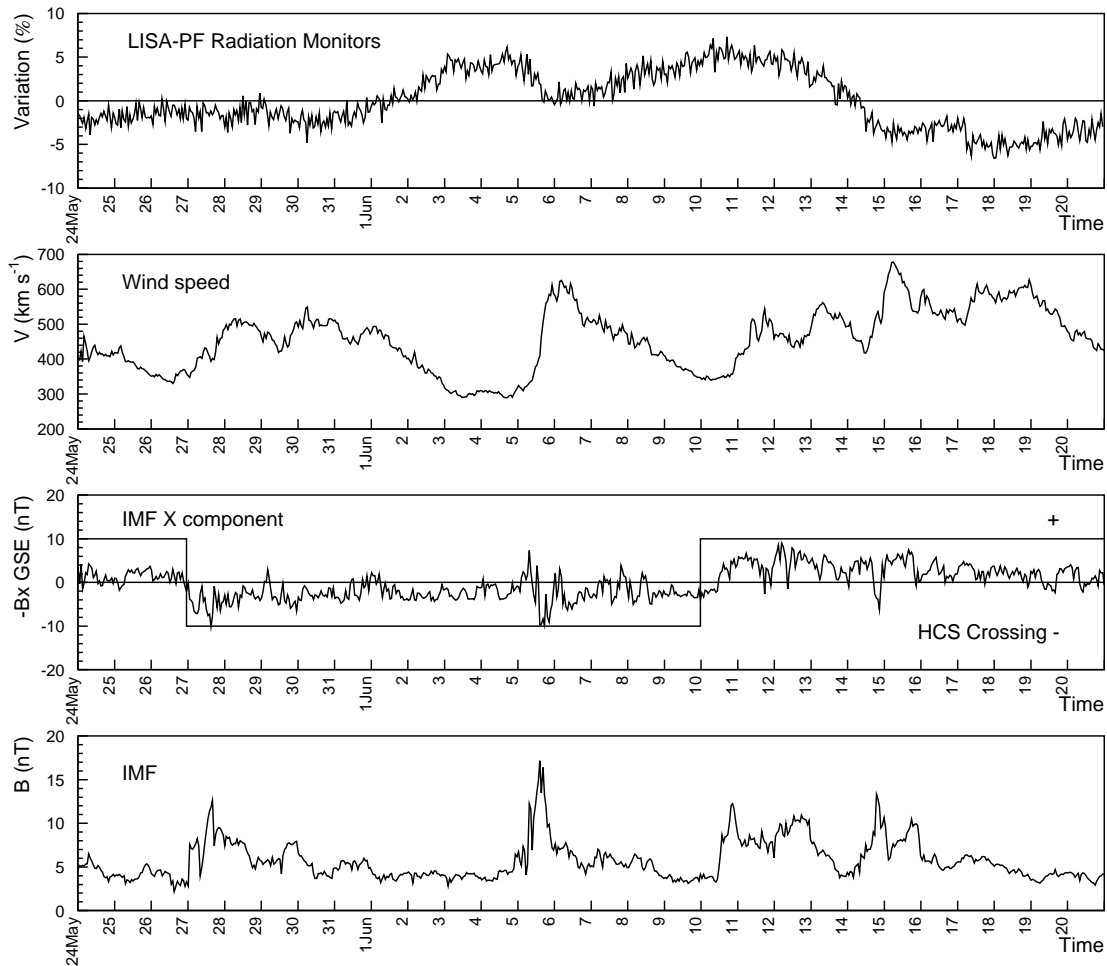


Figure 2. Same as Fig. 1 for the BR 2494 (May 24, 2016- June 20, 2016).

The average characteristics of recurrent GCR flux depressions observed in space with LPF and contemporaneously with polar neutron monitors are reported in Table 2. Neutron monitor data present a peaked distribution, while data in space show a flat distribution as it can be observed in Figs. 5 and 6 where the whole sample of the GCR flux recurrent variations observed in 2016-2017 with LPF are reported. In particular, it can be observed that while polar neutron monitors indicate maximum variations of approximately 4%, the same variations in space above 70 MeV n^{-1} are as large as more than 12%. The IP disturbances estimated to be at the origin of each one of these variations are reported in [Armano et al. \(2018a\)](#). In 87% of cases HSS transit only was associated

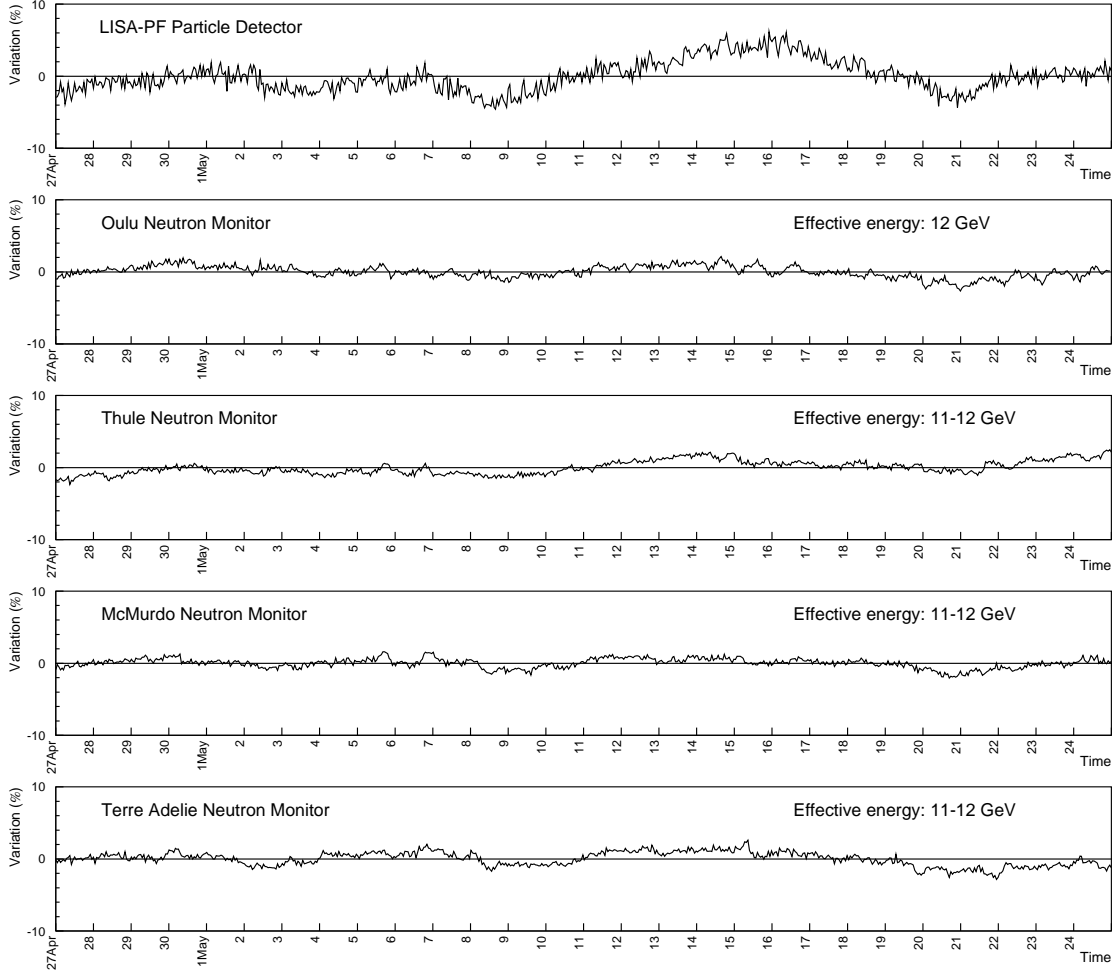


Figure 3. Comparison of hourly averaged LPF PD counting rate percent variations with contemporaneous, analogous measurements of polar neutron monitors during the BR 2493 (April 27, 2016 - May 23, 2016).

with recurrent GCR flux variations while the remaining 13% of cases HCSC and ICME transit contributed in modulating the GCR flux.

5. ENERGY DEPENDENCE OF RECURRENT SHORT-TERM GCR FLUX VARIATIONS WITH LISA PATHFINDER

Fourteen isolated leading edges and twelve trailing edges of HSS modulating the GCR flux were studied. HSS were considered isolated if their passage was separated by at least one day from other IP disturbances, during which the solar wind speed decreased down to or below $\simeq 400 \text{ km s}^{-1}$. One isolated HSS was observed, for instance, during the BR 2494 between June 4 and June 10, 2016 (see

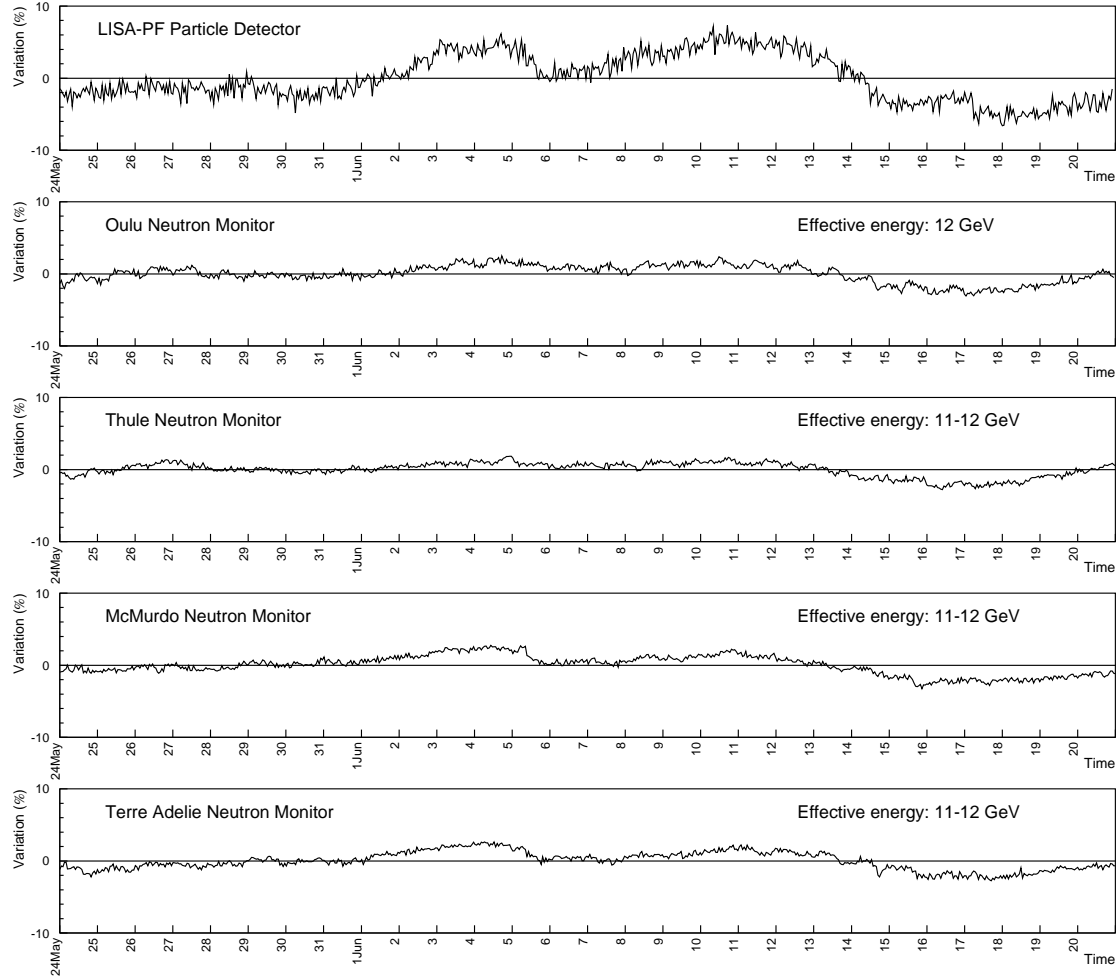


Figure 4. Same as Fig. 3 for the BR 2494 (May 24, 2016- June 20, 2016).

Fig. 2). In Fig. 7 solar wind speed variations above 400 km s^{-1} from the beginning through the dip of each GCR flux depressions are shown with the corresponding flux decrease amplitudes. In Fig. 8 twelve solar wind speed decreases down to 400 km s^{-1} and associated GCR flux recovery amplitudes are shown. In Fig. 7 (8) the solar wind speed and the GCR flux variations must be intended positive (negative) and negative (positive), respectively. On average, at the passage of individual HSS, the GCR flux is found to decrease by 4.4% with average solar wind speed increases of 226 km s^{-1} above 400 km s^{-1} . The most intense GCR intensity decreases are detected at the passage of IP disturbances if the GCR flux lies in the range $5\%-7\%$ above the average value observed during the corresponding BR. The smallest decreases are observed at the transit of IP structures in case the GCR flux is

Table 1. Energy dependence of the GCR integral flux percent change (PC) at the maximum of the six recurrent depressions observed on board LPF during the BRs 2493-2494 (see Figs. 3 and 4) above 70 MeV n^{-1} and with NMs above effective energies: 11-12 GeV for polar stations; 12 GeV for Oulu NM. Onset and dips of each depression were set according to the LPF data. Percentages were rounded to 0.5 percent.

LPF depression onset Time	LPF depression dip Time	LPF > 70 MeV PC	Terre Adelie > 11 GeV PC	McMurdo > 11 GeV PC	Thule > 11 GeV PC	Oulu > 12 GeV PC
2016 May 2 02.40 UT	2016 May 3 10.35 UT	3%	<1%	<1%	<1%	<1%
2016 May 6 18.45 UT	2016 May 8 13.20 UT	4.5%	2%	2%	1%	1%
2016 May 16 08.00 UT	2016 May 20 20.15 UT	8%	3%	2%	2%	2%
2016 May 29 01.00 UT	2016 May 30 10.50 UT	3%	<1%	<1%	<1%	<1%
2016 June 5 04.15 UT	2016 June 6 02.30 UT	4.5%	2.5%	2.5%	1.5%	1.5%
2017 June 12 13.15 UT	2016 June 17 22.25 UT	9.5%	3.5%	3.5%	3.5%	3.5%

Table 2. Average characteristics of GCR flux recurrent short-term depressions observed with LPF in space in 2016-2017. A comparison is carried out with contemporaneous GCR flux depression intensity observed with Earth polar NMs. GCR flux short-term variations gathered in space in 2016-2017 varied from 1.6% through 12.3% while on neutron monitors ranged from 1% to 4.1%. The average duration of the depressions observed with polar neutron monitors was not estimated due to the difficulty to establish the onset and end times of each GCR flux decrease.

	Duration (Days)	Intensity (%)
Space	9.2 ± 5.0	
Space		5.1 ± 2.5
Polar NMs	————	1.8 ± 1.6

already depressed. When the solar wind speed stops increasing but remains above 500 km s^{-1} the cosmic-ray flux does not recover. The recovery phases are characterized by average GCR intensity increases of 5.3% for mean solar wind speed decreases of 282 km s^{-1} .

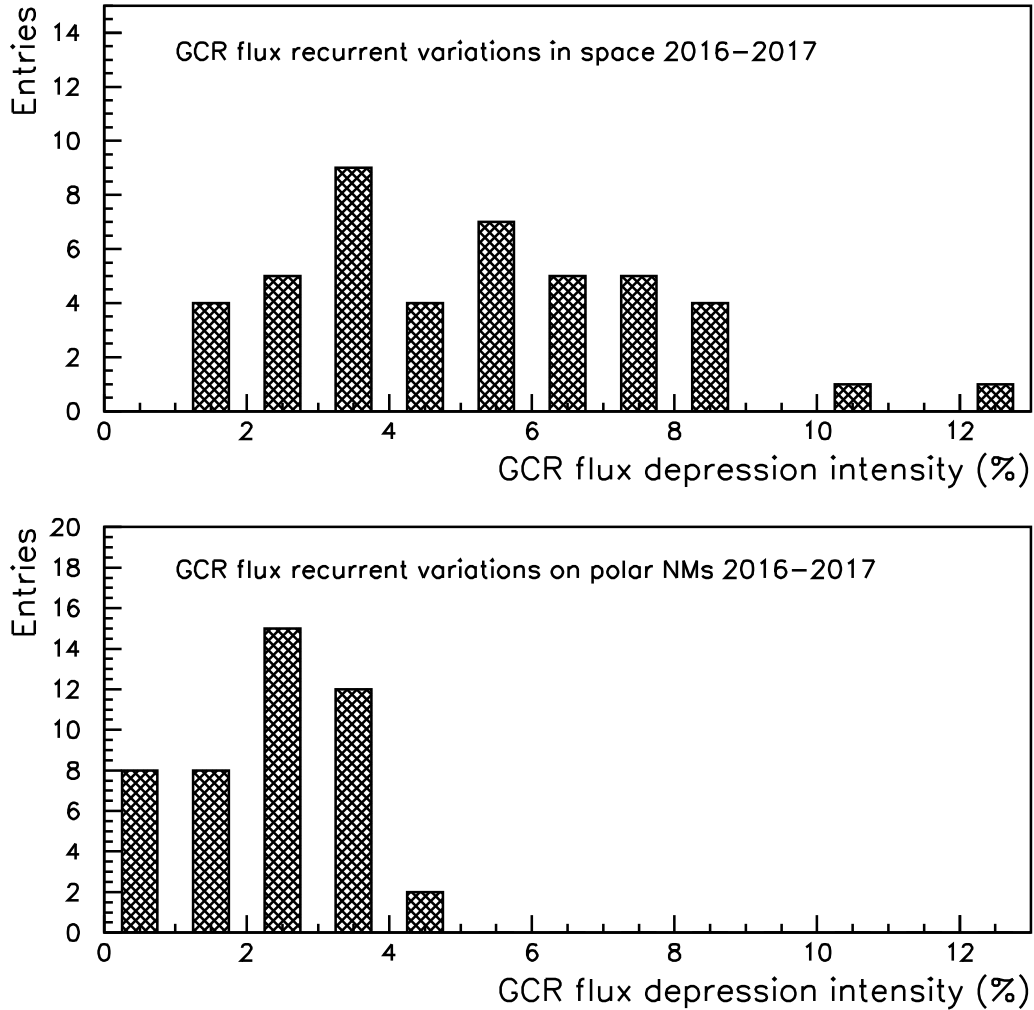


Figure 5. Comparison of GCR flux recurrent percent decreases observed in space on board LPF in 2016–2017 above 70 MeV n^{-1} (top panel) and on average on Earth with polar neutron monitors above 11 GeV n^{-1} (bottom panel).

In Fig. 9, the GCR depression commencement observed on November 21 during the BR 2500 is modulated by an isolated HSS.

In order to estimate the pre-decrease LPF proton-dominated differential flux and the differential flux at the dip of the depression on November 26–29, the proton AMS-02 measurements averaged during the same BR are considered first (Aguilar et al. 2018). Solid stars in Fig. 10 represent the AMS-02

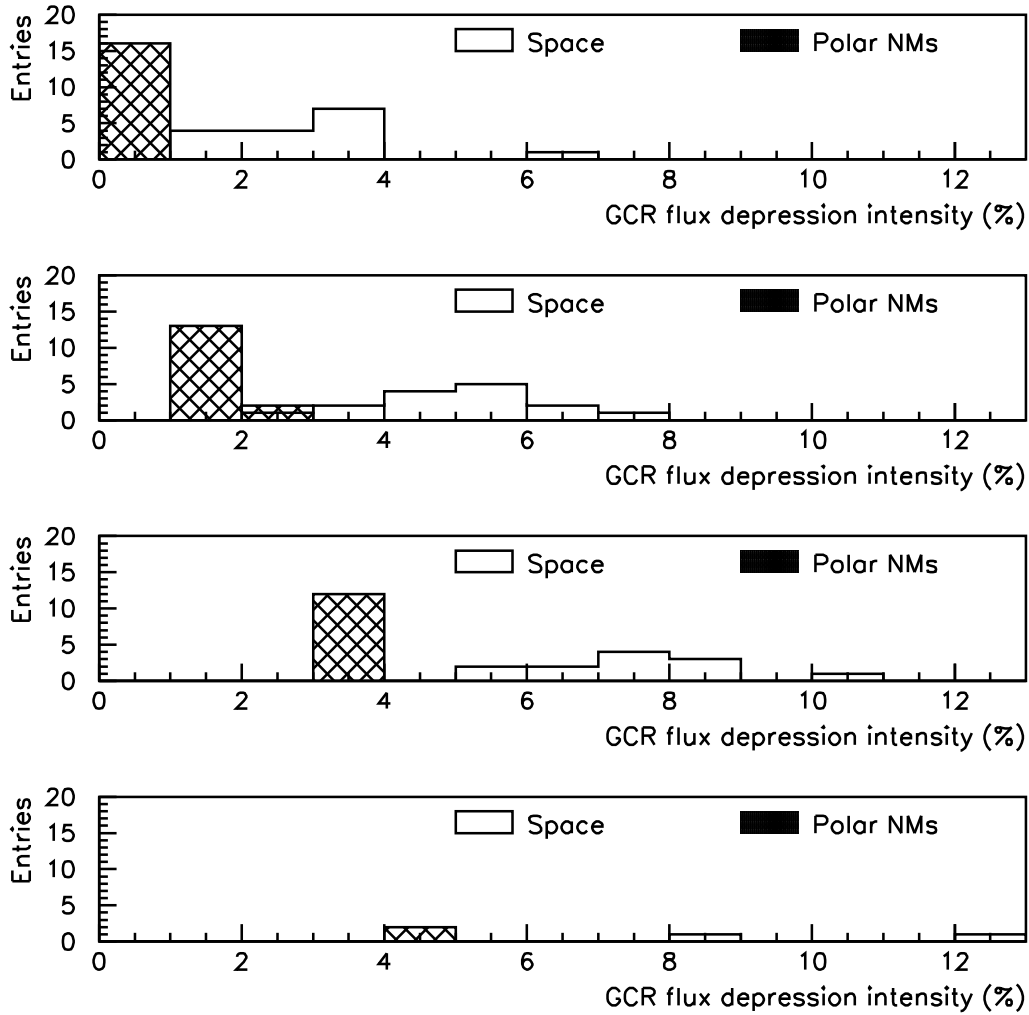


Figure 6. Comparison of GCR flux percent recurrent depressions observed on Earth polar neutron monitors (hatched area) in the intervals (0-1% - 1-3% - 3-4% 4-5% from top to bottom panels) with corresponding variations observed in space on board LPF in 2016-2017 (white area).

data and the dot-dashed line was obtained from the G&A model for a solar modulation parameter of 385 MV/c (November 2016). The proton interstellar spectrum by [Burger et al. \(2000\)](#) was used for this calculation. The model outcomes are interpolated according to the following equation down to 70 MeV n^{-1} :

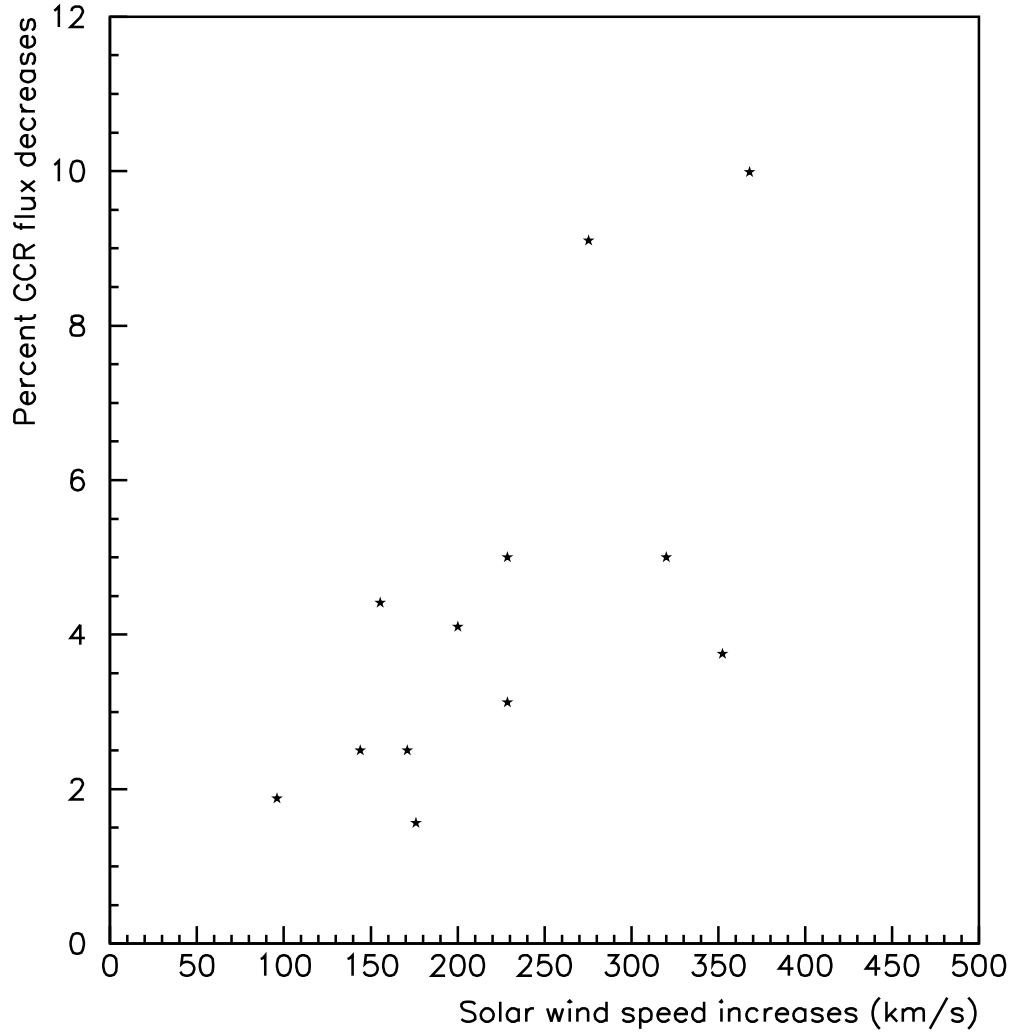


Figure 7. Solar wind speed increases and corresponding GCR flux percent decreases at the passage of HSSs in 2016-2017.

$$F(E) = A (E + b)^{-\alpha} E^{\beta} \quad \text{particles (m}^2 \text{ sr s GeV n}^{-1}\text{)}^{-1}, \quad (1)$$

found to well reproduce the model trend between tens of MeV and hundreds of GeV. In the above equation E is the particle kinetic energy per nucleon. The parameters A , b , α and β are reported in Table 3 (see [Armano et al. \(2018a\)](#) for details) for the dot-dashed line and for the top and bottom continuous lines of Fig. 10. The parameter A represents the spectrum normalization while the

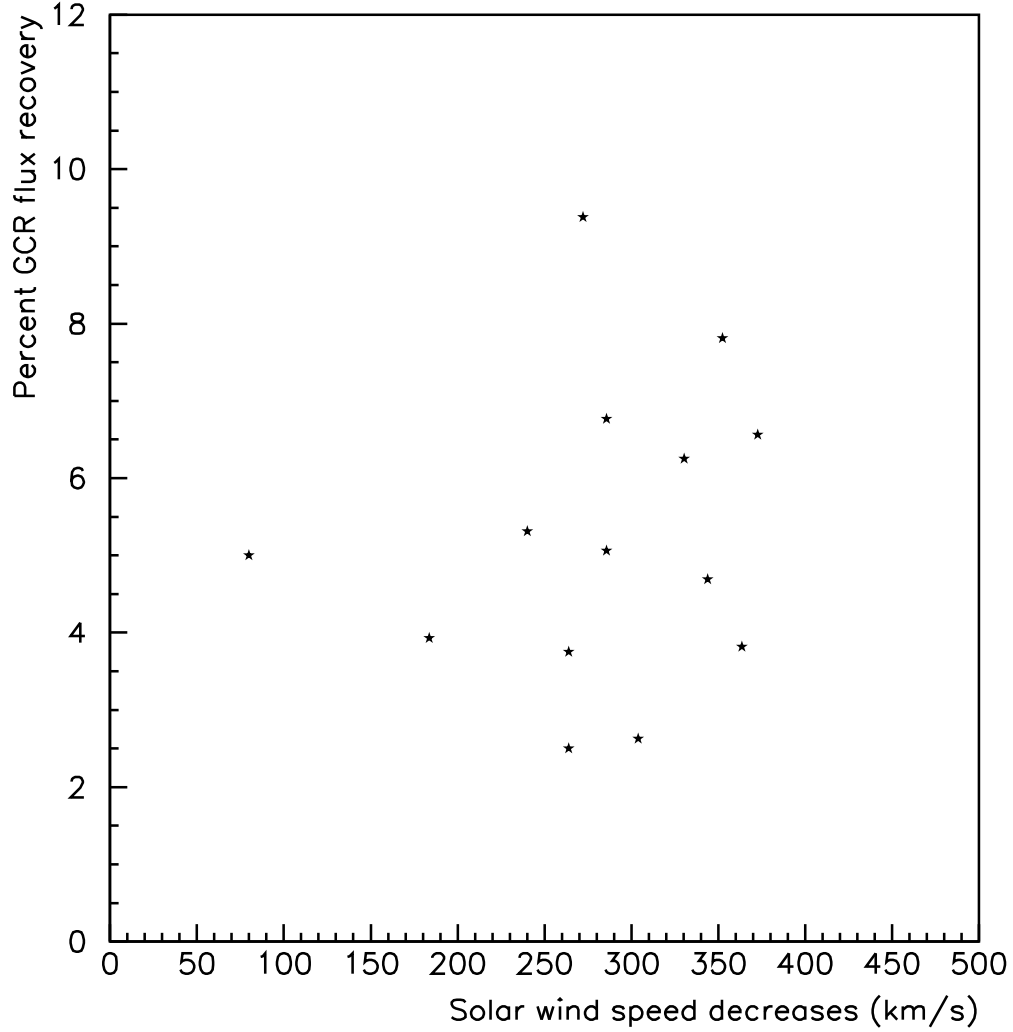


Figure 8. Solar wind decreases and corresponding GCR flux percent recoveries in 2016-2017.

parameter b determines the spectrum modulation below a few GeV. The parameters α and β set the spectrum slope at high energies. By increasing the parameter b the spectrum maintains the same spectral index at high energies but is modulated below a few GeV. It is worthwhile to point out that this parameterization is used only for the purpose of reproducing the trend of the experimental data and for the G&A model outcome parameterization. The parameter values are set on this basis only and no physical meaning must be assigned. The same approach was used to study the energy dependence of FDs in [Armano et al. \(2018a, 2019\)](#). The continuous lines represent the GCR flux

on November 20, 2016 (top line) and on November 26-29, 2016 (bottom line). These differential proton fluxes were obtained by taking into account that on November 20 the LPF GCR proton dominated integral flux was observed to be +5.5% above the value averaged during the BR 2500 and on November 26-29, 3% below. The proton flux at the dip of the depression appears modulated mainly below 2 GeV, as it results from Fig. 11 where it can be observed that polar NMs above 11 GeV show a variation of about 1%. Differential proton-dominated fluxes are inferred, and consequently the parameter b is set, by requiring that the integral fluxes above 70 MeV and 11 GeV are consistent with the LPF and NMs measurements. These observations mark a difference with GCR flux modulation during FDs of similar intensities observed with LPF (Armano et al. 2019) for which polar and high latitude neutron monitors showed a variation of 4% and 2%, respectively. It is pointed out that the uncertainty of neutron monitor measurements on hourly averaged data is well below 1%. In Figs. 12 and 13 the energy dependence of GCR flux variations show that the flux does not recover until the very last few days of the BR 2503 while neutron monitor observations do not show any evident variation.

The GCR flux remains close to its average value estimated during an entire BR either if the solar wind speed remains below 400 km s^{-1} or well above 500 km s^{-1} . In the first case the GCR flux is at its maximum value during the studied BR. In the second, the GCR flux is depressed. We can assess that when a large sample of GCR short-term variation evolutions down to a few tens of MeV will be observed in space on board the future space interferometers for gravitational waves and, possibly, other instruments before the LISA launch, more will be known about differences in the energy dependence of recurrent and non recurrent GCR flux variations. These findings must be correctly taken into account to carry out precise estimates of instrument performance in space. For instance, the role of GCR energy differential flux variations in generating spurious noise force due to the charging process of free-falling metal test-masses of the LISA interferometer represents the main concern about mission performance below 10^{-3} Hz . The ESA Next Generation Radiation Monitors (Desorgher et al. 2013) will be flown on each LISA spacecraft. This detector consists of two units, one for 2-200 MeV proton and one for 100 keV-7 MeV electron monitoring. This detector is

optimized for solar energetic particle event detection and short-term forecast. However, the detector performance in the energy range of cosmic rays is quite poor. It was recently proposed to fly on LISA a third particle detector unit, similar to that located on board of LPF. This third unit may consist of only one silicon detector of $2.8 \times 2.8 \text{ cm}^2$ area placed inside a copper box stopping particles below 70 MeV s^{-1} . This unit, possibly oriented with its viewing axis perpendicularly to the nominal Parker spiral direction, would allow to monitor hourly GCR short-term variations within 1% uncertainty.

6. RECURRENT GALACTIC COSMIC-RAY FLUX VARIATIONS AND GEOMAGNETIC ACTIVITY IN 2016-2017

In [Grimani et al. \(2019b\)](#) it was explored the possibility to use three weak FDs (July 20, 2016, August 2, 2016, May 27, 2017) observed on board LPF as proxies for non-recurrent geomagnetic activity associated with the arrival at the Earth of the associated ICMEs. It was observed that FDs could have been used for forecasting intense geomagnetic storms only when a negative B_z component (in Geocentric Solar Ecliptic (GSE) coordinate system) of the IP magnetic field reconnecting with the Earth's magnetic field was assuming values smaller than -20 nT and the interplanetary magnetic field intensity was $> 20 \text{ nT}$. However, in [Telloni et al. \(2020\)](#) it was shown that if the solar wind energy is large enough, geomagnetic activity is observed also when the B_z of the IP magnetic field is northern. To this purpose, recurrent depressions of the GCR flux observed with LPF and recurrent geomagnetic activity are discussed.

The association between corotating solar wind streams and weak to moderate recurrent geomagnetic activity was discussed in [Tsurutani et al. \(2006\)](#). It is recalled here that a weak geomagnetic activity is correlated with the disturbance storm time (Dst) geomagnetic index ranging between -30 nT and -50 nT , while the geomagnetic activity is considered moderate in case the Dst varies between -50 nT and -100 nT . Weak-moderate geomagnetic activity in 2016-2017 during the time LPF remained into orbit was observed when the B_z component of the IP magnetic field presented values $< -12 \text{ nT}$. However, weak-moderate geomagnetic activity was also observed at the leading edge of fast solar wind streams characterized by minimum speeds ranging between 550 km s^{-1} and 650 km s^{-1} and a region of enhanced plasma pressure of at least 12 nPa regardless of the B_z value. Recurrent

Table 3. Parameterizations of proton energy spectra averaged over the BR 2500, before and at the dip of the depression started on November 22, 2016.

	A	b	α	β
AMS-02 proton flux	18000	1.15	3.66	0.92
Pre-decrease proton flux	18000	1.115	3.66	0.92
Proton flux at the depression dip	18000	1.172	3.66	0.92

geomagnetic activity was associated with passage of HSS from the BR 2491 through the BR 2494 on March 16-17, 2016 (Dst \simeq -50 nT), April 13-14, 2016 (Dst \simeq -55 nT), May 8-9, 2016 (Dst \simeq -80 nT) and June 5-6, 2016 when the geomagnetic activity became weak (Dst \simeq -40 nT). Analogously, recurrent geomagnetic activity was also observed on September 1-2, 2016 (Dst \simeq -60 nT), September 29, 2016 (Dst \simeq -60 nT) and October 25, 2016 (Dst \simeq -50 nT) from BR 2497 through BR 2499 . The weak to moderate geomagnetic activity is always associated with GCR flux recurrent variations in L1. It must be pointed out, however, that GCR flux depressions due to the interplay of closely spaced HSS (< 1 day) characterized by solar wind speed > 400 km s $^{-1}$ cannot trigger geomagnetic activity because of a small solar wind energy with typical flow pressure of just a few nPa (Telloni et al. 2020).

GCR short-term variation observations in L1 not only help in disentangling long and short term variations of the GCR flux but also represent a precious proxy of weak to moderate geomagnetic activity.

7. CONCLUSIONS

The energy differential flux of GCRs during the evolution of individual recurrent short-term variations has been studied by comparing data gathered in deep space with the ESA mission LPF, with cosmic-ray dedicated experiments in space and with polar NMs. The passage of HSS of similar characteristics are associated with GCR depression amplitudes differing by more than a factor of two depending if the particle flux was close to minimum or maximum values during each BR before the passage of modulating HSS. An almost constant cosmic-ray flux is observed when the solar wind speed remains below 400 km s $^{-1}$ or above 500 km s $^{-1}$. In the first case the GCR flux is at its maxi-

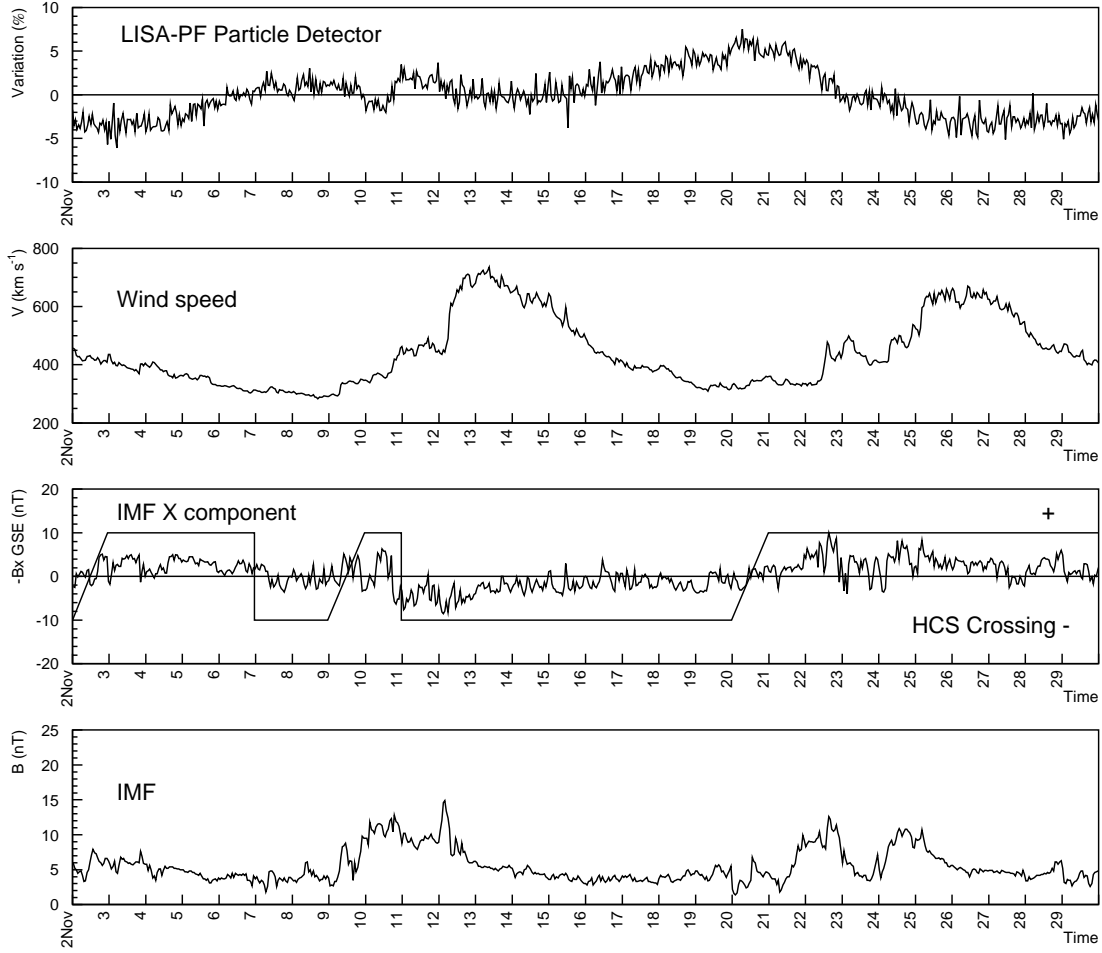


Figure 9. Same as Fig. 1 for the BR 2500 (November 2, 2016 - November 28, 2016).

mum value for the period of the solar cycle and solar polarity. In the second case, the flux is steadily depressed by the passage of closely spaced HSS. The GCR flux during recurrent short-term depressions presented maximum amplitudes of about 12% in 2016-2017 and resulted modulated mainly below 2 GeV while during FDs of the same amplitude, and energy dependence of several percent was observed above 10 GeV.

GCR flux depressions in L1 are good proxies to monitor weak to moderate geomagnetic activity being both processes associated with the passage of corotating HSS. The only exception is associated with the transit of several HSS when the solar wind speed does not decrease at 400 km s^{-1} and the GCR flux is already depressed. In this case, the formation of regions of enhanced pressure $> 12 \text{ nPa}$

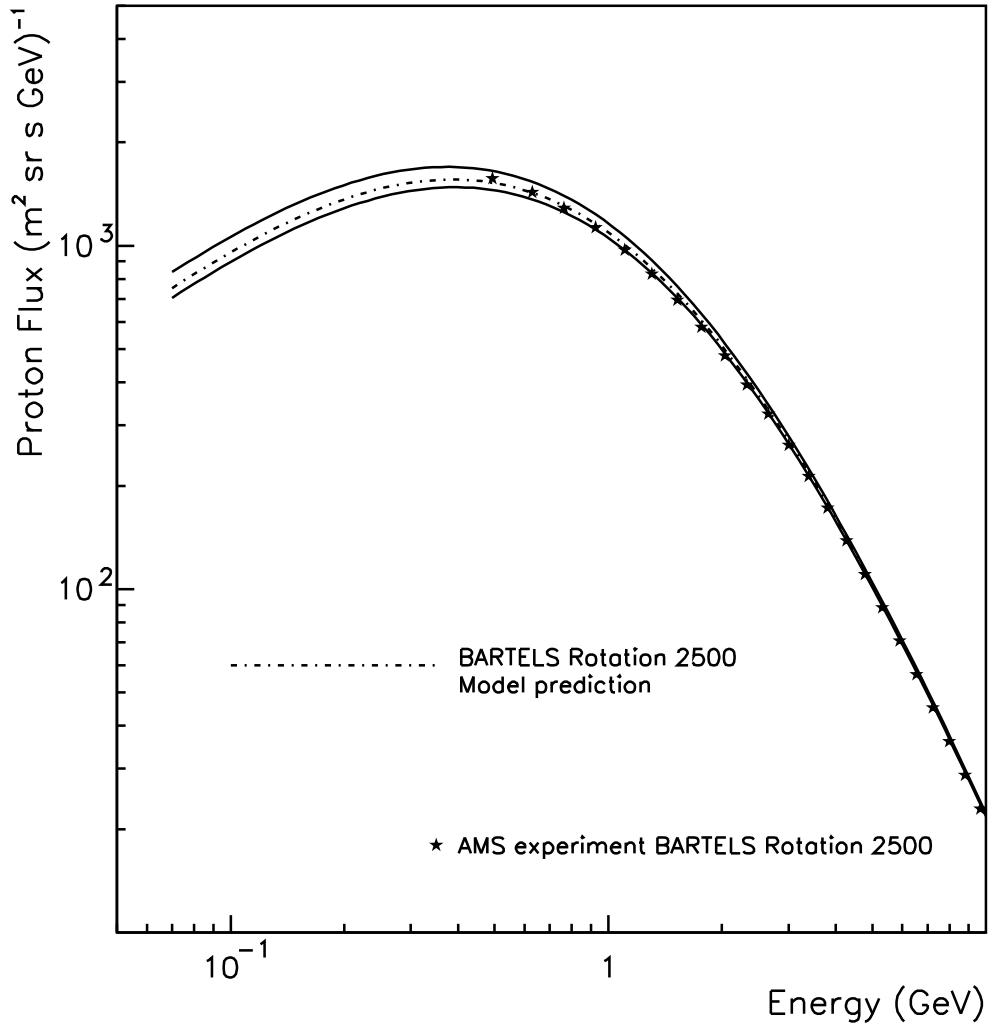


Figure 10. Energy dependence of the GCR proton dominated flux depression commenced on November 20, 2016 (top continuous line) during the BR 2500 on board LPF. The bottom continuous line represents the same flux at the maximum of the depression on November 26-29 2016. The dot-dashed line shows the average GCR proton flux during the BR 2500 resulting from the interpolation (equation 1) of the AMS-02 experiment data (solid stars).

is impeded and consequently the solar wind energy is not large enough to disturb the geomagnetic field regardless of the B_z value.

ACKNOWLEDGEMENTS

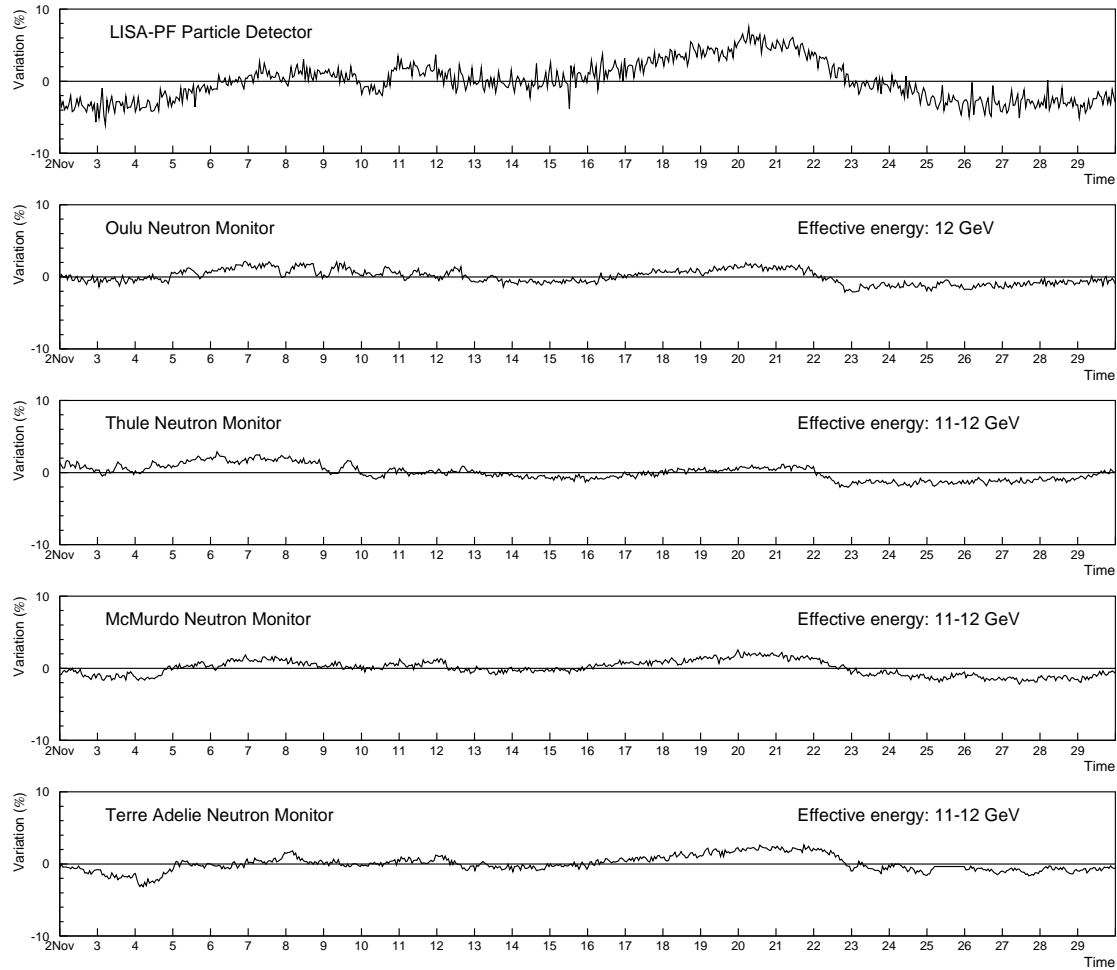


Figure 11. Same as Fig. 2 for the BR 2500 (November 2, 2016 - November 29, 2016).

The LISA Pathfinder cosmic-ray data can be downloaded from <https://www.cosmos.esa.int/web/lisa-pathfinder-archive/home>. Sunspot number data were gathered from <http://www.sidc.be/silso/home>. Data from ACE and Wind experiments are taken from the NASA-CDAWeb website. The ICME catalog appears in <http://www.srl.caltech.edu/ACE/ASC/DATA/level3/icmetable2.htm>. NMs data are gathered from www.nmdb.eu. The authors thank the PIs of the NM network.

REFERENCES

- | | |
|--|---|
| <p>Adriani, O., Barbarino, G. C., Bazilevskaya, G. A., et al. 2011, <i>The Astrophysical Journal</i>, 742, 102, doi: 10.1088/0004-637x/742/2/102</p> | <p>Adriani, O., Barbarino, G. C., Bazilevskaya, G. A., et al. 2018, <i>ApJL</i>, 852, L28, doi: 10.3847/2041-8213/aaa403</p> |
|--|---|

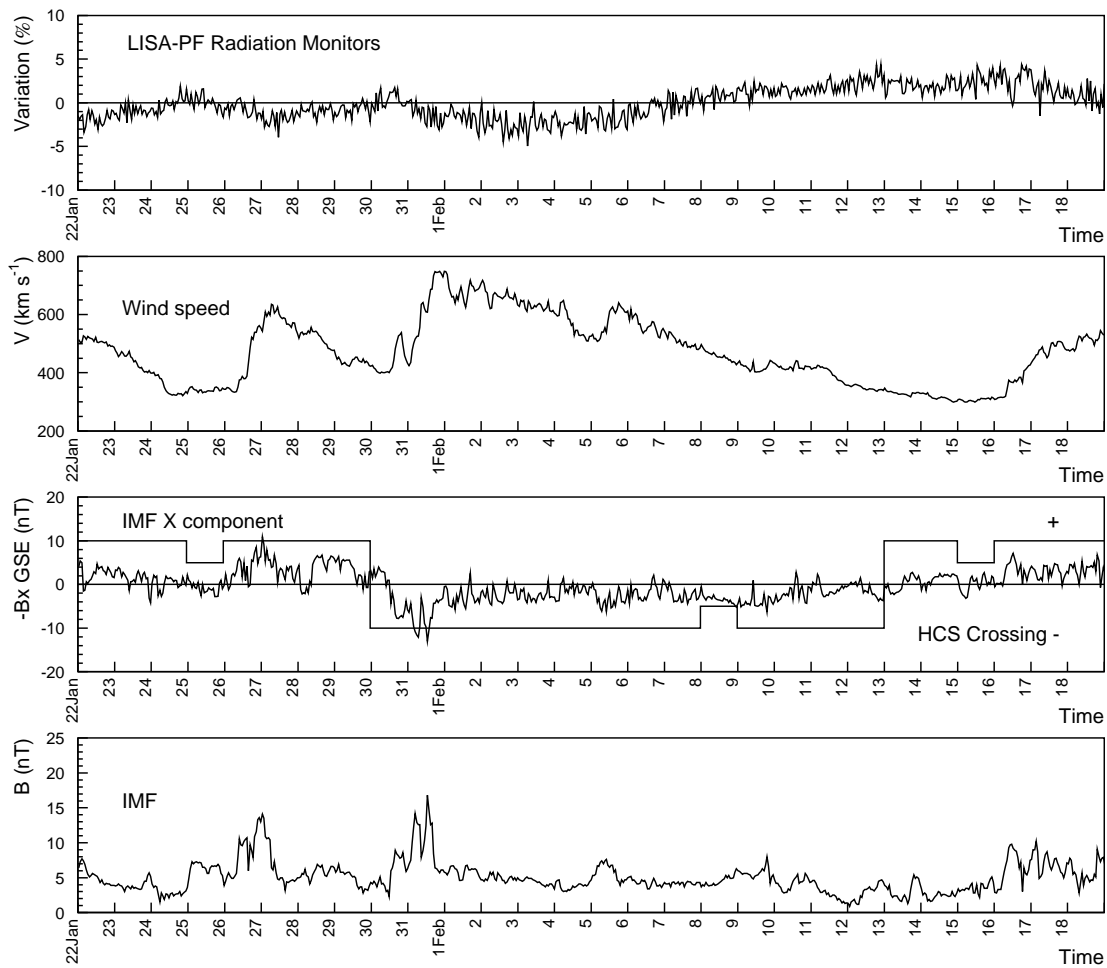


Figure 12. Same as Fig. 1 for BR 2503 (January 22, 2016- February 17, 2016).

Aguilar, M., Ali Cavazonza, L., Alpat, B., et al.

2018, *Phys. Rev. Lett.*, 121, 051101,

doi: [10.1103/PhysRevLett.121.051101](https://doi.org/10.1103/PhysRevLett.121.051101)

Amaro-Seoane, P., Audley, H., Babak, S., et al.

2017, arXiv e-prints, arXiv:1702.00786.

<https://arxiv.org/abs/1702.00786>

AMS Collaboration, Aguilar, M., Alcaraz, J.,

et al. 2002, *PhR*, 366, 331,

doi: [10.1016/S0370-1573\(02\)00013-3](https://doi.org/10.1016/S0370-1573(02)00013-3)

Andretta, V., Bemporad, A., Focardi, M., et al.

2014, in *Society of Photo-Optical*

Instrumentation Engineers (SPIE) Conference

Series, Vol. 9152, Software and

Cyberinfrastructure for Astronomy III, 91522Q,

doi: [10.1117/12.2055158](https://doi.org/10.1117/12.2055158)

Antonucci, E., Romoli, M., Andretta, V., et al.

2019, *Astronomy & Astrophysics*,

doi: [10.1051/0004-6361/201935338](https://doi.org/10.1051/0004-6361/201935338)

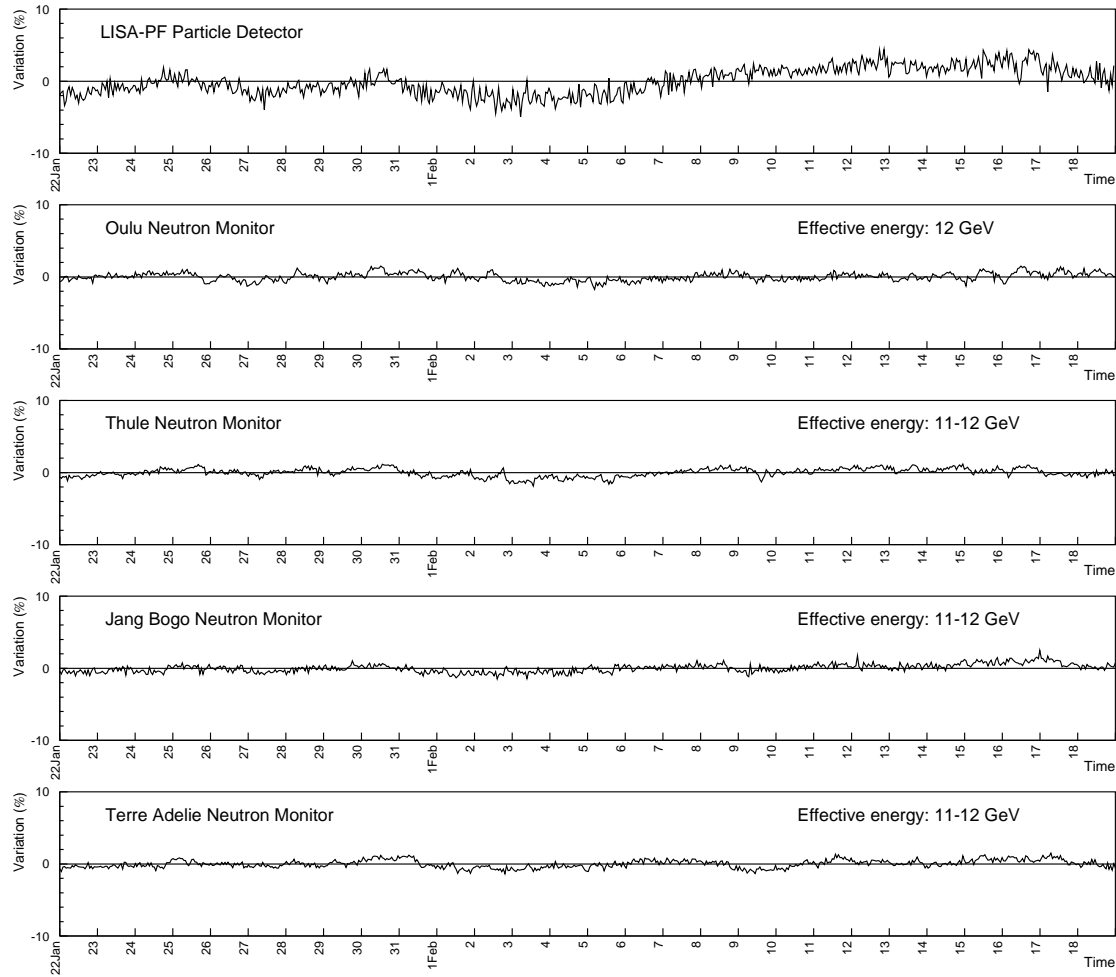


Figure 13. Same as Fig. 2 for BR 2503 (January 22, 2016- February 17, 2016).

Antonucci, F., Armano, M., Audley, H., et al.

2011, *Classical and Quantum Gravity*, 28,
094002, doi: [10.1088/0264-9381/28/9/094002](https://doi.org/10.1088/0264-9381/28/9/094002)

—. 2012, *Classical and Quantum Gravity*, 29,
124014, doi: [10.1088/0264-9381/29/12/124014](https://doi.org/10.1088/0264-9381/29/12/124014)

Araujo, H. M., Wass, P., Shaul, D., Rochester, G.,
& Sumner, T. J. 2005, *Astropart. Phys.*, 22,
451, doi: [10.1016/j.astropartphys.2004.09.004](https://doi.org/10.1016/j.astropartphys.2004.09.004)

Armano, M., Audley, H., Auger, G., et al. 2016,
Phys. Rev. Lett., 116, 231101,
doi: [10.1103/PhysRevLett.116.231101](https://doi.org/10.1103/PhysRevLett.116.231101)

—. 2017, *Phys. Rev. Lett.*, 118, 171101,
doi: [10.1103/PhysRevLett.118.171101](https://doi.org/10.1103/PhysRevLett.118.171101)

Armano, M., Audley, H., Baird, J., et al. 2018a,
Astrophys. J., 854, 113,
doi: [10.3847/1538-4357/aaa774](https://doi.org/10.3847/1538-4357/aaa774)

—. 2018b, *Phys. Rev. Lett.*, 120, 061101,
doi: [10.1103/PhysRevLett.120.061101](https://doi.org/10.1103/PhysRevLett.120.061101)

—. 2018c, *Astroparticle Physics*, 98, 28,
doi: [10.1016/j.astropartphys.2018.01.006](https://doi.org/10.1016/j.astropartphys.2018.01.006)

—. 2019, *Astrophys. J.*, 874, 167,
doi: [10.3847/1538-4357/ab0c99](https://doi.org/10.3847/1538-4357/ab0c99)

- Balogh, A. 1998, *SSRv*, 83, 93
- Benella, S., Grimani, C., Fabi, M., Finetti, N., & Villani, M. 2019a, *International Cosmic Ray Conference*, 36, 76
- Benella, S., Grimani, C., Laurenza, M., & Consolini, G. 2019b, *Nuovo Cimento C Geophysics Space Physics C*, 42, 44, doi: [10.1393/ncc/i2019-19044-7](https://doi.org/10.1393/ncc/i2019-19044-7)
- Benella, S., Laurenza, M., Vainio, R., et al. 2020, *ApJ*, 901, 21
- Burger, R. A., Potgieter, M. S., & Heber, B. 2000, *Journal of Geophysical Research: Space Physics*, 105, 27447, doi: [10.1029/2000JA000153](https://doi.org/10.1029/2000JA000153)
- Cane, H. V. 2000, *SSRv*, 93, 55, doi: [10.1023/A:1026532125747](https://doi.org/10.1023/A:1026532125747)
- Canizares, P., Chmeissani, M., Conchillo, A., et al. 2011, *Classical and Quantum Gravity*, 28, 094004, doi: [10.1088/0264-9381/28/9/094004](https://doi.org/10.1088/0264-9381/28/9/094004)
- Corti, C., Potgieter, M. S., Bindi, V., et al. 2019, *ApJ*, 871, 253, doi: [10.3847/1538-4357/aafac4](https://doi.org/10.3847/1538-4357/aafac4)
- de Simone, N., di Felice, V., Gieseler, J., et al. 2011, *Astrophysics and Space Sciences Transactions*, 7, 425, doi: [10.5194/astra-7-425-2011](https://doi.org/10.5194/astra-7-425-2011)
- Desorgher, L., Hajdas, W., Britvitch, I., et al. 2013, in *2013 14th European Conference on Radiation and Its Effects on Components and Systems (RADECS)*, 1–5
- Florinski, V., & Pogorelov, N. V. 2009, *ApJ*, 701, 642, doi: [10.1088/0004-637X/701/1/642](https://doi.org/10.1088/0004-637X/701/1/642)
- Florinski, V., Zank, G. P., & Pogorelov, N. V. 2003, *Journal of Geophysical Research: Space Physics*, 108, doi: [10.1029/2002JA009695](https://doi.org/10.1029/2002JA009695)
- Forbush, S. E. 1937, *Physical Review*, 51, 1108, doi: [10.1103/PhysRev.51.1108.3](https://doi.org/10.1103/PhysRev.51.1108.3)
- . 1954, *Journal of Geophysical Research*, 59, 525, doi: [10.1029/JZ059i004p00525](https://doi.org/10.1029/JZ059i004p00525)
- . 1958, *Journal of Geophysical Research*, 63, 651, doi: [10.1029/JZ063i004p00651](https://doi.org/10.1029/JZ063i004p00651)
- Gil, A., Asvestari, E., Kovaltsov, G., & Usoskin, I. 2017, in *International Cosmic Ray Conference, Vol. 301, 35th International Cosmic Ray Conference (ICRC2017)*, 32
- Gleeson, L. J., & Axford, W. I. 1968, *Ap. J.*, 154, 1011
- Grimani, C., Benella, S., Fabi, M., et al. 2019a, *Nuovo Cimento C Geophysics Space Physics C*, 42, 42, doi: [10.1393/ncc/i2019-19042-9](https://doi.org/10.1393/ncc/i2019-19042-9)
- Grimani, C., Fabi, M., Lobo, A., Mateos, I., & Telloni, D. 2015, *Classical and Quantum Gravity*, 32, 035001, doi: [10.1088/0264-9381/32/3/035001](https://doi.org/10.1088/0264-9381/32/3/035001)
- Grimani, C., Telloni, D., Benella, S., et al. 2019b, *Atmosphere*, 10, 749, doi: [10.3390/atmos10120749](https://doi.org/10.3390/atmos10120749)
- Grimani, C., et al. 2007, in *30th International Cosmic Ray Conference (Merida)*
- Jokipii, J. R., Levy, E. H., & Hubbard, W. B. 1977, *ApJ*, 213, 861, doi: [10.1086/155218](https://doi.org/10.1086/155218)
- Martucci, M., Munini, R., Boezio, M., et al. 2018, *ApJL*, 854, L2, doi: [10.3847/2041-8213/aaa9b2](https://doi.org/10.3847/2041-8213/aaa9b2)

- McCracken, K. G., Rao, U. R., & Bukata, R. P. 1966, *PhRvL*, 17, 928, doi: [10.1103/PhysRevLett.17.928](https://doi.org/10.1103/PhysRevLett.17.928)
- Modzelewska, R., Bazilevskaya, G., Boezio, M., et al. 2019, in *International Cosmic Ray Conference*, Vol. 36, 36th International Cosmic Ray Conference (ICRC2019), 1128
- Munini, R., Boezio, M., Bruno, A., et al. 2018, *ApJ*, 853, 76, doi: [10.3847/1538-4357/aaa0c8](https://doi.org/10.3847/1538-4357/aaa0c8)
- Pamela Collaboration, Adriani, O., Barbarino, G. C., et al. 2017, *Nuovo Cimento Rivista Serie*, 40, 473, doi: [10.1393/ncr/i2017-10140-x](https://doi.org/10.1393/ncr/i2017-10140-x)
- Potgieter, M. S. 2013, *SSRv*, 176, 165, doi: [10.1007/s11214-011-9750-7](https://doi.org/10.1007/s11214-011-9750-7)
- Richardson, I. G. 2004, *SSRv*, 111, 267, doi: [10.1023/B:SPAC.0000032689.52830.3e](https://doi.org/10.1023/B:SPAC.0000032689.52830.3e)
- Richardson, I. G., Wibberenz, G., & Cane, H. V. 1996, *J. Geophys. Res.*, 101, 13483, doi: [10.1029/96JA00547](https://doi.org/10.1029/96JA00547)
- Rodriguez-Pacheco, J., Wimmer-Schweingruber, R. F., Mason, G. M., et al. 2019, *Astronomy & Astrophysics*, doi: [10.1051/0004-6361/201935287](https://doi.org/10.1051/0004-6361/201935287)
- Sabbah, I. 2000, *Geophys. Res. Lett.*, 27, 1823, doi: [10.1029/2000GL003760](https://doi.org/10.1029/2000GL003760)
- Shaul, D. N. A., et al. 2006, *AIP Conf. Proc.*, 873, 172
- Shikaze, Y., Haino, S., Abe, K., et al. 2007, *Astroparticle Physics*, 28, 154, doi: [DOI:10.1016/j.astropartphys.2007.05.001](https://doi.org/10.1016/j.astropartphys.2007.05.001)
- Stone, E. C., Cummings, A. C., McDonald, F. B., et al. 2013, *Science*, 341, 150, doi: [10.1126/science.1236408](https://doi.org/10.1126/science.1236408)
- Storini, M. 1990, *Nuovo Cimento C Geophysics Space Physics C*, 13, 103, doi: [10.1007/BF02515780](https://doi.org/10.1007/BF02515780)
- Telloni, D., Fabi, M., Grimani, C., & Antonucci, E. 2016, *AIP Conference Proceedings*, 1720, doi: <http://dx.doi.org/10.1063/1.4943856>
- Telloni, D., Carbone, F., Antonucci, E., et al. 2020, *ApJ*, 896, 149, doi: [10.3847/1538-4357/ab91b9](https://doi.org/10.3847/1538-4357/ab91b9)
- Tsurutani, B. T., Gonzalez, W. D., Gonzalez, A. L. C., et al. 2006, *Journal of Geophysical Research (Space Physics)*, 111, A07S01, doi: [10.1029/2005JA011273](https://doi.org/10.1029/2005JA011273)
- Usoskin, I. G., Bazilevskaya, G. A., & Kovaltsov, G. A. 2011, *Journal of Geophysical Research (Space Physics)*, 116, A02104, doi: [10.1029/2010JA016105](https://doi.org/10.1029/2010JA016105)
- Usoskin, I. G., Gil, A., Kovaltsov, G. A., Mishev, A. L., & Mikhailov, V. V. 2017, *Journal of Geophysical Research (Space Physics)*, 122, 3875, doi: [10.1002/2016JA023819](https://doi.org/10.1002/2016JA023819)
- Villani, M., Benella, S., Fabi, M., & Grimani, C. 2020, *Applied Surface Science*, 512, 145734, doi: [10.1016/j.apsusc.2020.145734](https://doi.org/10.1016/j.apsusc.2020.145734)